Missouri State University

BearWorks

College of Natural and Applied Sciences

1-1-2013

Effective charge collection in dye-sensitized nanocrystalline TiO_2

Masatoshi Yanagida

Youhei Numata

Keiichi Yoshimatsu

Shin Satoh

Liyuan Han

Follow this and additional works at: https://bearworks.missouristate.edu/articles-cnas

Recommended Citation

Yanagida, Masatoshi, Youhei Numata, Keiichi Yoshimatsu, Shin Satoh, and Liyuan Han. "Effective charge collection in dye-sensitized nanocrystalline TiO2." Advances in Natural Sciences: Nanoscience and Nanotechnology 4, no. 1 (2013): 015006.

This article or document was made available through BearWorks, the institutional repository of Missouri State University. The work contained in it may be protected by copyright and require permission of the copyright holder for reuse or redistribution.
For more information, please contact BearWorks@library.missouristate.edu.

OPEN ACCESS
IOP PUBLISHING
ADVANCES IN NATURAL SCIENCES: NANOSCIENCE AND NANOTECHNOLOGY
Adv. Nat. Sci.: Nanosci. Nanotechnol. **4** (2013) 015006 (8pp)
doi:10.1088/2043-6262/4/1/015006

Effective charge collection in dye-sensitized nanocrystalline TiO_2

Masatoshi Yanagida[1,2], Youhei Numata[2], Keiichi Yoshimatsu[2], Shin Satoh[2] and Liyuan Han[2]

[1] Global Research Center for Environment and Energy based on Nanomaterials Science (GREEN), National Institute of Materials Science, 1-2-1 Sengen, Tsukuba, Ibaraki 305-0047, Japan
[2] Photovoltaic Materials Research Unit, National Institute of Materials Science, 1-2-1 Sengen, Tsukuba, Ibaraki 305-0047, Japan

E-mail: YANAGIDA.Masatoshi@nims.go.jp

Received 15 October 2012
Accepted for publication 31 December 2012
Published 29 January 2013
Online at stacks.iop.org/ANSN/4/015006

Abstract
The effective charge collection in dye-sensitized solar cells (DSCs) is an important factor to improve the efficiency. Here, we report the comparison of three types of structures in DSCs. One type of structure is a sandwich-type DSC (SW-DSC), in which the TiO_2 film is sandwiched between a TCO glass front electron-collection electrode and a sputtered Ti back collection electrode. The second is a normal DSC (N-DSC), which has no back electrode. The third is a back-contact-type DSC (BC-DSC), in which a sputtered Ti back electrode is deposited on a TiO_2 film on the opposite side of the normal glass as an optical window. The photocurrent response of an SW-DSC is the fastest of the three structures due to using intensity modulated photocurrent spectroscopy, which can be explained by the electron diffusion model. The model shows that the SW-DSC is a favorable structure for effective charge collection in DSCs.

Keywords: dye-sensitized solar cells, nanocrystalline, TiO_2, electron transport, charge collection

Classification number: 2.07

1. Introduction

The charge transport in nanocrystalline semiconductor film electrodes has attracted considerable scientific interest [1–11]. The nanocrystalline TiO_2 film electrode consists of sintering 5–400 nm diameter particles on a transparent conductive oxide (TCO) glass, and has especially been utilized for dye-sensitized solar cells (DSCs). Normal DSCs (N-DSCs) generally consists of a dye-sensitized nanocrystalline TiO_2 film, an electrolyte solution containing an I_3^-/I^- redox couple, and a counter electrode (figure 1(a)). The thickness of the nanocrystalline TiO_2 film is about 10–30 μm. Because of its large surface area, the light harvesting efficiency of this film can be 100%, even when dyes adsorbs on TiO_2 surface at the monolayer [1–9].

N-DSCs are illuminated with solar light from the TCO side, whereupon the excited dye injects an electron into the nanocrystalline TiO_2, and the resulting oxidized dye is reduced by an I^- ion in the electrolyte. The photo-generated electron diffuses in the TiO_2, eventually arrives at, and is collected by the TCO glass, which acts as a charge-collection electrode. The photoresponse of the short-circuit photocurrent density (J_{SC}) in N-DSCs is much slower (micro- to milliseconds) than that of classical inorganic semiconductor devices (nano- to picoseconds). The application of DSCs to commercial devices such as photovoltaics, photo-detector and sensor will be limited by the slow photoresponse. Two explanations for this slow photoresponse have been proposed. One is the slow electron diffusion in nanocrystalline TiO_2. The electron diffusion coefficient ($<10^{-3}$ cm^2 s^{-1}) is much smaller than that in single-crystalline TiO_2 (0.01 cm^2 s^{-1}) [10, 11]. Nanocrystalline TiO_2 has shallow energy trap sites (around 10^{18} cm^{-3}) or potential barrier (distance 6 nm) of grain boundary among the TiO_2 particles [12–22]. The electrons in the conduction band therefore move very slowly through nanocrystalline TiO_2. The second explanation for the slow photoresponse involves the position of the extraction electrode

© 2013 Vietnam Academy of Science & Technology

Original content from this work may be used under the terms of the Creative Commons Attribution 3.0 licence. Any further distribution of this work must maintain attribution to the author(s) and the title of the work, journal citation and DOI.

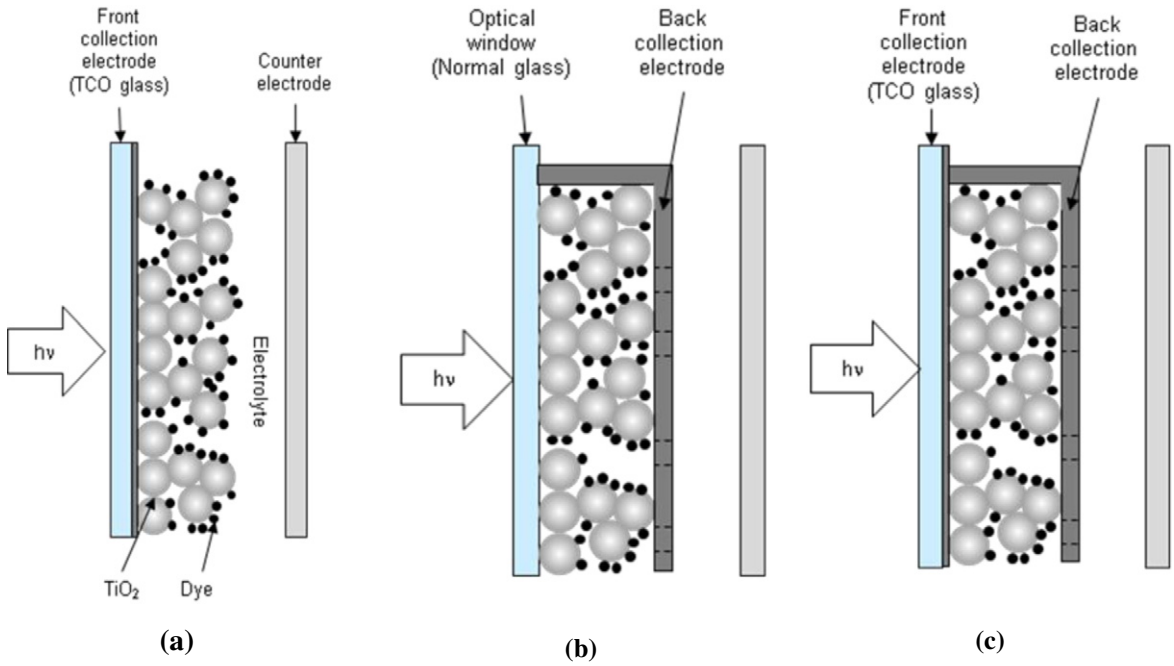

Figure 1. Structure of (a) normal DSCs (N-DSCs), (b) back contact-type DSCs (BC-DSCs) and (c) sandwich contact-type DSCs (SW-DSCs).

and the interfacial area between the extraction electrode and the TiO_2 film. The TCO glass serves not only as a light window but also as the front-collection electrode. Recently, the back contact-type DSC (BC-DSC), in which a charge collection electrode is placed on the TiO_2 film on the side opposite the optical window [23–37] has been proposed in order to remove highly costly TCO, and to improve the J_{SC} without reflection loss on the TCO layer (figure 1(b)).

In N-DSCs, the electrons are initially generated by irradiated light around TCO, and exponentially decrease from TCO to the counter electrode. In BC-DSC, the electrons are initially generated by irradiated light around the optical window (normal glass), and exponentially decrease from the optical window to the collection electrode. The distance between photo-generated part and the collection part in BC-DSCs is longer than that in N-DSCs. We expected that the photocurrent response of BC-DSCs is slower than that of N-DSCs. We recently showed the photocurrent response of sandwich contact-type DSCs (SW-DSCs) as shown in figure 1(c) [38]. The back collection electrode was placed on nanocrystalline TiO_2 film opposite the TCO glass. To investigate the effect of the position of the collection electrode on the photocurrent density, we evaluated photocurrent density of N-, BC- and SW-DSCs by measuring the photocurrent frequency response, as well as by calculating the incident monochromatic photon-to-current conversion efficiency (IPCE) response by means of an electron diffusion model.

2. Experiment

2.1. Materials

All chemicals were obtained from Wako Pure Chemical Industries (Osaka, Japan), Tokyo Chemical Industry Co. (Tokyo, Japan), or Sigma-Aldrich Japan Co. (Tokyo, Japan), and were used as supplied. N719 dye, TiO_2 pastes and TCO glass substrates were purchased from Dyesol (Queanbeyan, Australia).

2.2. DSC fabrication

Nanocrystalline TiO_2 photoelectrodes for the N-, BC- and SW-DSCs were prepared as follows [38]. TCO and normal glass substrates were washed with acetone, 37% hydrochloric acid and distilled water under ultrasonic irradiation for 30 min; and they were washed again with acetone and distilled water under ultrasonic irradiation for 30 min just prior to TiO_2 film fabrication. Nanocrystalline TiO_2 thin films were screen-printed onto the glass substrates. The thickness of the TiO_2 film was measured with a micro-figure measuring instrument (Surfcorder ET4000, Kosaka Laboratory, Tokyo, Japan). The thickness of the TiO_2 films used for this study was 9.7 μm (20 nm particle layer). For the BC- and SW-DSCs, we deposited Ti as the back electrode on the TiO_2 film by using a sputtering machine (Ulvac Technologies, Chigasaki, Japan) under a vacuum of 7.8×10^{-2} Torr under a flow of Ar gas (20 sccm). The TiO_2-coated substrates were dipped into an acetonitrile/*tert*-butylalcohol (1 : 1 v/v) solution of N719 dye (3 mM) and heated for 70 h at 35 °C for adsorption of the dyes onto the TiO_2 surface. The coated substrates were clipped together with a platinized glass counter electrode with pin holes. The gap between the two electrodes was sealed with a thermal adhesive film (Surlyn-50 MS004620, Dyesol). Then an electrolyte consisting of 0.6 mM 1-methyl-3-propylimidazolium iodide, 0.1 mM LiI, 0.2 mM *tert*-butylpyridine and 0.05 mM I_2 in acetonitrile was injected into the gap.

2.3. Characterization of the DSCs

The *J–V* characteristics of the DSCs were measured with a WXS-90S-L2 super solar simulator (Wacom, Tokyo,

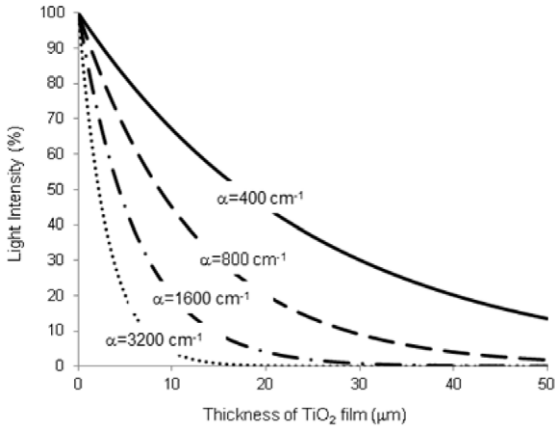

Figure 2. Absorption coefficient (α) dependent light absorption profile in nanocrystalline TiO_2 films sensitized with dye.

Japan) under air mass 1.5 simulated solar illumination at 100 mW cm^{-2}. IPCE spectra were measured with a CEP-200BX spectrometer (Bunkokeiki, Tokyo, Japan). DSC devices with an active surface area of 0.25 cm^2 were created by means of a metal mask [39, 40].

Intensity modulated photocurrent spectroscopy was performed with a red diode laser (NEOARK, 650 nm, 35 mW) under short circuit condition. The power of modulated-light irradiation was reduced to <10% of the total photocurrent of the DSCs. When the frequency of the modulated-light irradiation was changed from 10 mHz to 100 kHz, the resulting changes in the amplitude and phase of the small sinusoidal voltage were detected with an impedance analyzer (Solartron 1255B) [17, 38].

3. Results and discussion

3.1. Light absorption profile

The calculated absorption profile in a nanocrystalline TiO_2 film sensitized with dyes is shown in figure 2. The light absorption is linearly related to the light intensity. The light absorption is largest at the optical window ($x = 0$ in figure 2). The light intensity exponentially decreases with an increase of thickness of TiO_2 The light absorption in TiO_2 film can be expressed as the following:

$$I(x) = I_0 \exp(-\alpha x), \tag{1}$$

where x is the distance (cm) from the optical window in TiO_2 films, $I(x)$ is light intensity at x, α is absorption coefficient (cm^{-1}) and I_0 is incident light intensity, respectively. Equation (1) is well known as Lambert–Beer law. Because the electron is generated by the absorbed photon, the electron generated by photon is distributed around optical windows. In case of large α, the generated electron distributes around $x = 0$. The probability of the collection by the collection electrode is large in N-DSC. The average distance (AD) between the position of a generated electron and a collection electrode in an N-DSC is very small because an electron is generated around the TCO glass. The probability of the collection in a BC-DSC is small because AD in BC-DSCs should be longer than that in N-DSCs. In the case of small α, the generated electrons widely distribute in the TiO_2 film. The AD in an N-DSC becomes larger. But AD in a BC-DSC becomes smaller. The electron collection in a BC-DSC should become favorable. On the other hand, the AD should be constant in an SW-DSC. The collection electrodes exist on both sides.

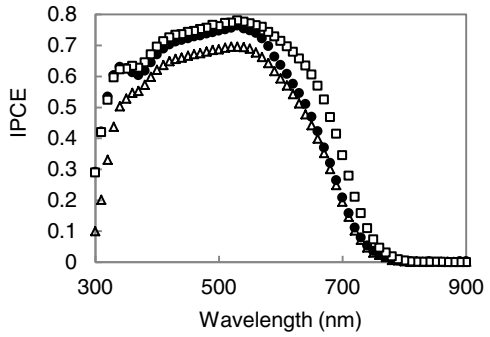

Figure 3. Incident monochromatic photon to current conversion efficiency (IPCE) spectra of an N-DSC(□), a BC-DSC(△) and an SW-DSC(●).

3.2. Photovoltaic properties

We evaluated the photovoltaic properties of the SW- and N-DSCs. The short circuit current (J_{SC}), open circuit voltage (V_{OC}) and fill factor (FF) values of the N-DSC were 14.0 mA cm^{-2}, 0.751 V and 0.720, respectively; and the corresponding values of the BC-DSC were 10.9 mA cm^{-2}, 0.779 V and 0.767. In the SW-DSC, J_{SC}, V_{OC} and FF were 11.8 mA cm^{-2}, 0.761 V and 0.728, respectively. The overall conversion efficiencies of the N-, BC- and SW-DSCs were 7.6, 6.5 and 6.6%, respectively.

Incident monochromatic photon-to-current conversion efficiency (IPCE) spectra of an N-DSC, a BC-DSC and an SW-DSC are shown in figure 3. The maximum IPCE of the SW-DSC was comparable to that of the N-DSC. However, J_{SC} of the SW-DSC was slightly lower than that of the N-DSC, owing to light absorption by the back collection electrode at wavelengths > 600 nm. In an N-DSC, light reflected and scattered by the counter electrode can impinge upon the TiO_2 film again. In contrast, in an SW-DSC and a BC-DSC, light transmitted through the TiO_2 film is immediately absorbed on the Ti back electrode. The loss of the reflected and scattered light reduced the J_{SC} value of the SW-DSC and the BC-DSC relative to that of the N-DSC.

In the BC-DSC, the maximum IPCE was lowest of the three different types of DSC. We now investigate the reason for the low J_{SC}. The total AD of BC-DSCs may be smallest. The optical properties of the optical window may also be changed when we change from a TCO glass to a normal glass.

3.3. Photocurrent frequency response

We normalized the IPCE of these DSCs at 650 nm to the value of the N-DSCs and investigated its dependence upon the frequency of applied modulating light (figure 4). The corrected IPCE response gradually decreased, starting at a frequency of around 20 Hz and decreasing to nearly 0 at frequencies >10 kHz. At a frequency of around 100 Hz, the IPCE response increased with increasing electron density (n)

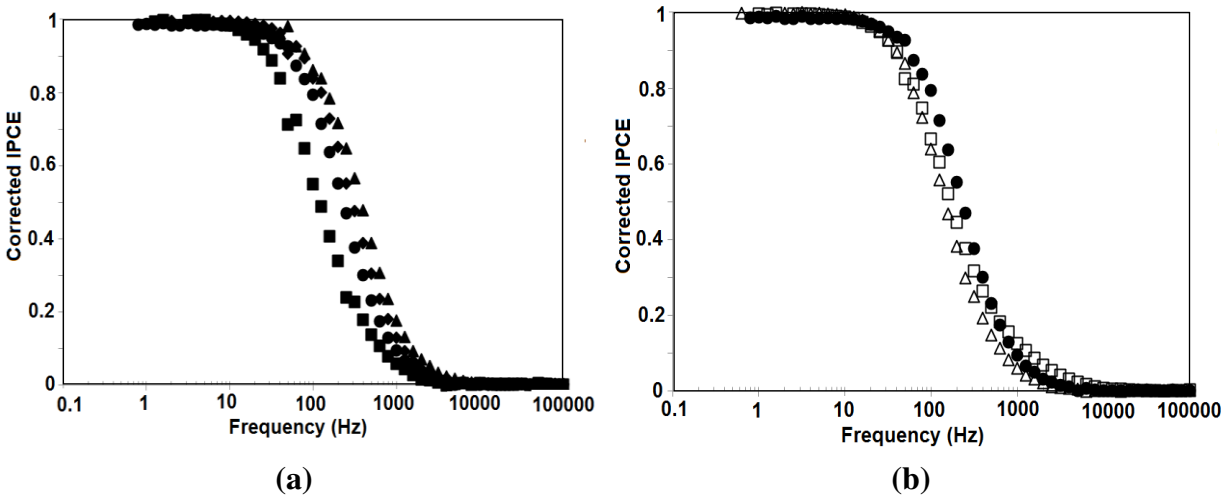

Figure 4. Corrected photocurrent response as a function of frequency of applied modulating light at 650 nm. (a) Electron density (n) dependent photocurrent response of a SW-DSC. The response at $n = 2.9 \times 10^{17}$ (■), 5.0×10^{17} (●), 5.7×10^{17} (♦), 6.6×10^{17} cm^{-3} (▲). The n at open circuit condition was measured by the charge extraction method under different irradiation powers. (b) Corrected photocurrent response of an N-DSC (□), a BC-DSC(△) and an SW-DSC(●) at $n = 5.0 \times 10^{17}$ cm^{-3}.

in TiO_2 (figure 4(a)). The electron density was measured by the charge extraction method at various light intensities [13, 14]. When electrons in TiO_2 diffuse in nanocrystalline TiO_2, the electrons are trapped and de-trapped thorough electron trap sites. The D value in TiO_2 films is smaller than that of bulk crystalline TiO_2. However, the number of electrons in TiO_2 increases with increasing light intensity, and these electrons fill up the traps. As a result, additional electrons can move smoothly through the conduction band without undergoing trapping and de-trapping. Therefore, the IPCE response increases with increasing n.

The corrected IPCE response becomes larger in the order of SW- > N- > BC-DSCs at frequencies from 10 to 500 Hz (figure 4(b)). Because the same TiO_2, N719 dye, electrolyte and counter electrode were used in both types of DSCs, the photovoltaic properties (e.g. D, τ and α) in the three types of DSCs can be expected to be identical. Therefore, the faster response of the IPCE in the SW-DSCs was likely to have been due to the addition of the back collection electrode. The difference in photocurrent response of these DSCs decreased with increasing light intensity. Because D increases with increasing light intensity, electrons in TiO_2 can be quickly collected by the front electrode at high light intensities, even when the back or the front electrode is not present.

At frequencies > 500 Hz, the IPCE response of the SW-DSCs was smaller than that of the N-DSCs. The response at frequencies > 500 Hz was not due to electron diffusion and can instead be explained in terms of the influence of the attenuation factor (AF(ω)), which is explained later [11].

The photocurrent density (J_{SC}) can be explained by using the electron diffusion model. We defined that the collection electrode existed at $x = 0$ in N-DSCs or BC-DSCs, at $x = 0$ and d in SW-DSCs when we consider the TiO_2 films with thickness of d. When DSCs are illuminated from the optical window, the density ($n(x,t)$) of electrons in TiO_2 is a function of the distance (x) from the interface between the optical window and the nanocrystalline TiO_2 and time (t) and is given by the following continuity equation [10–15]:

$$\frac{\partial n\,(x,t)}{\partial t} = D\frac{\partial^2 n\,(x,t)}{\partial x^2} - \frac{n\,(x,t)}{\tau} + \alpha I_0 \mathrm{e}^{-\alpha y}, \qquad (2)$$

where D is the electron diffusion coefficient, τ is the electron lifetime, y is $d - x$ in BC-DSCs and x in N-DSCs or SW-DSCs, respectively. The J_{SC} can be described as the gradient of n value at the interface between a TiO_2 film and a collection electrode

$$J_{SC} = qD\frac{\partial n\,(x_C,t)}{\partial x} \quad (x_C = 0 \text{ or } d), \qquad (3)$$

where q is the quantity of charge on the electron.

Equation (2) can be solved under the boundary condition of each DSC. We can define the condition at the interface between a TiO_2 film and a collection electrode as the following equation:

$$k_e n(x_C,t) = D\frac{\partial n\,(x_C,t)}{\partial x} \quad (x_C = 0 \text{ or } d), \qquad (4)$$

where k_e is the rate constants of the electron collection from TiO_2 to the collection electrode. The distribution of electron at interface between a TiO_2 film and an insulated optical window or an electrolyte can be defined as the following equation:

$$\frac{\partial n\,(x_O,t)}{\partial x} = 0 \quad (x_O = 0 \text{ or } d). \qquad (5)$$

In the case of N-DSCs and BC-DSCs, we use $x_O = d$ in equation (5) and $x_C = 0$ in equations (3) and (4). In the case of SW-DSCs, we use both $x_C = 0$ and d in equations (3) and (4), but need not use equation (5).

From equations (2), (4) and (5), the distribution of electron density (n) against x can be calculated, and then J_{SC} is calculated from each gradient of $n(x)$ at the interface between a collection electrode and a TiO_2 film as shown in equation (3). Finally, we can calculate the photocurrent (IPCE) frequency response $J(\omega)$, which can be described as the following:

$$J(\omega) = qDu'(\omega), \qquad (6)$$

Table 1. List of equations for photocurrent response $J(\omega)$.

Type of cells	u′ (ω)	A	B	C
N-DSC	$-\gamma A_N$	$A_N = C/\gamma$	$B_N = -C/\gamma$	
	$+\gamma B_N$	$[\{(k_e + D\gamma)\alpha - (k_e - D\alpha)\gamma e^{-\gamma d}\}$	$[\{(k_e - D\gamma)\alpha + (k_e - D\alpha)\gamma e^{\gamma d}\}$	
	$+\alpha C$	$/\{k_e(e^{\gamma d} + e^{-\gamma d}) + D\gamma(e^{\gamma d} - e^{-\gamma d})\}]$	$/\{k_e(e^{\gamma d} + e^{-\gamma d}) + D\gamma(e^{\gamma d} - e^{-\gamma d})\}]$	
BC-DSC	γA_{BC}	$A_{BC} = -Ce^{-\alpha d}/\gamma$	$B_{BC} = Ce^{-\alpha d}/\gamma$	$\alpha I_0/\{D(\gamma^2 - \alpha^2)\}$
	$-\gamma B_{BC}$	$[\{(k_e + D\gamma)\alpha e^{\alpha d} + (k_e - D\alpha)\gamma e^{-\gamma d}\}$	$[\{(k_e - D\gamma)\alpha e^{\alpha d} - (k_e - D\alpha)\gamma e^{\gamma d}\}$	
	$+\alpha C e^{-\alpha d}$	$/\{k_e(e^{\gamma d} + e^{-\gamma d}) + D\gamma(e^{\gamma d} - e^{-\gamma d})\}]$	$/\{k_e(e^{\gamma d} + e^{-\gamma d}) + D\gamma(e^{\gamma d} - e^{-\gamma d})\}]$	
SW-DSC	$(1 + e^{\gamma d})\gamma A_{sw}$	$A_{SW} = C$	$B_{SW} = -C$	
	$+(1 + e^{-\gamma d})\gamma B_{SW}$	$[\{(k_e + D\alpha)(e^{-\alpha d} - 2e^{\gamma d} + e^{-\gamma d})\}$	$[\{(k_e + D\alpha)(e^{-\alpha d} - e^{\gamma d})\}$	
	$+(1 + e^{-\alpha d})\alpha C$	$/\{(k_e - D\gamma)(e^{\gamma d} - e^{-\gamma d})\}]$	$/\{(k_e + D\gamma)(e^{\gamma d} - e^{-\gamma d})\}]$	

In these equations, $\gamma = \{(D\tau)^{-1} + (i\omega/D)\}^{1/2}$, where i is $(-1)^{1/2}$.

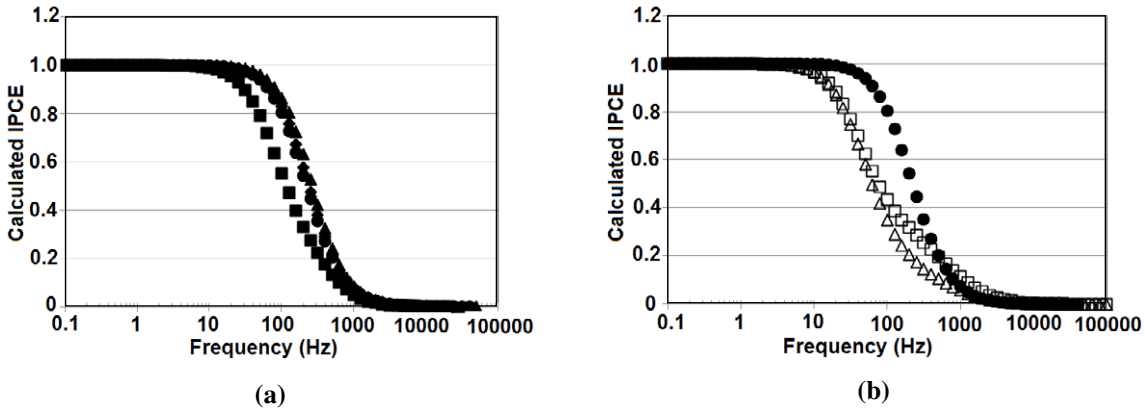

Figure 5. Calculated photocurrent response as a function of frequency of applied modulating light. (a) D dependence of calculated photocurrent response for SW-DSCs at $D = 2.5 \times 10^{-4}$ (■), 5×10^{-4} (●) and 2×10^{-3} cm^2 s^{-1} (▲), (b) Calculated photocurrent response of an N-DSC(□), a BC-DSC(△) and an SW-DSC(●) at $D = 5 \times 10^{-4}$. The following parameter values were used for the calculations: $d = 10\,\mu$m, $R = 3\,\Omega$, $k_{ext} = 10$ cm s^{-1}, $\alpha = 823$ cm^{-1}, $\tau = 1$ s.

where ω is frequency of modulated light. The equation of $u'(\omega)$ and the related parameters are summarized in table 1 [11, 38].

The observed photocurrent response $J_{app}(\omega)$ in the intensity modulated photocurrent spectra is attenuated by the attenuation factor AF(ω) [11]:

$$J_{app}(\omega) = \mathrm{AF}(\omega)\ J(\omega), \tag{7}$$

AF(ω) is given by

$$\mathrm{AF}(\omega) = \frac{1}{1 + i\omega RC}, \tag{8}$$

where i is $(-1)^{1/2}$, R is the series resistance of the sheet resistance of the collection electrode and the electrolyte and C is capacitance, which depends on the surface area of the collection electrode and TiO_2 film in the DSC. The plot of $J_{app}(\omega)$ versus ω is shown in figure 5. When D value increases as shown in figure 5(a), the $J_{app}(\omega)$ becomes large. The collection electrode can collect electrons, when electrons fast diffuse in TiO_2. The relationship between calculated $J_{app}(\omega)$ and D is in good agreement with the results in figure 4(a). As shown in figure 5(b), the $J_{app}(\omega)$ becomes larger in the order of SW- > N- > BC-DSCs at frequencies from 10 to 500 Hz, which is in agreement with the experimental results (figure 4(b)). In good agreement between figures 4 and 5, the diffusion model can be applied for prediction of the properties of N-, BC- and SW-DSCs.

3.4. Photocurrent density at steady state

At steady state under illumination, the diffusion equation (2) can be described as the following [10]:

$$0 = D\frac{\partial^2 n\,(x, t = \infty)}{\partial x^2} - \frac{n\,(x, t = \infty)}{\tau} + \alpha I_0 e^{-\alpha y}. \tag{9}$$

We defined n_0 as the electron density in TiO_2 under dark conditions. When we solve equation (9) by using Laplace transform and the boundary condition of equations (4) and (5), we can get the equation of the electron density ($n(x, t = \infty)$) in steady state, and J_{SC} for N-, BC- and SW-DSCs [10, 38]. In SW-DSCs, electrons generated in the TiO_2 diffuse to both the front and the back collection electrodes. The electrons in TiO_2 are separately collected by the front and back electrodes. But the collected electrons at both sides finally flow through the same outer circuit. Therefore, we assumed that the total current density can be expressed as the sum of the current densities at the front electrode and the back electrode for a given TiO_2 thickness d. These equations for n and J_{SC} are summarized in table 2. When we input the parameters such as α, d, D and τ into these equations in table 2, we can simulate $n(x, t = \infty)$ in TiO_2 at short circuit condition, and J_{SC}.

The calculation of $n(x, t = \infty)$ in TiO_2 are shown in figure 6. The α, d, n_0, D and τ values used for the calculations were 823 cm^{-1}, 10 μm, 10^{13} cm^{-3}, 5×10^{-4} cm^2 s^{-1}, and 1 s, respectively. In figure 6, light is irradiated from $x = 0$.

Table 2. List of the equations for the electron density $n(x, t = \infty)$ in steady state and short circuit photocurrent (J_{SC}).

Type of cells	$n(x, t = \infty)$	J_{SC}
N-DSC	$n_0\{1 - \cosh(x/L)\}$ $+P[Z(x) - LZ'(x = d)\sinh(x/L)/\cosh(d/L)]$	$qDPZ'(x = d)/\cosh(d/L)$
BC-DSC	n_0 $+P[Y(x) - LY'(x = d)\sinh(x/L)/\cosh(d/L)]$	$-qDPY'(x = d)/\cosh(d/L)$
SW-DSC	n_0 $+P[Z(x) - LZ(x = d)\sinh(x/L)/\sinh(d/L)]$	$qDP[Z'(x = d) - Z(x = d)\{\cosh(d/L) - 1\}/$ $\{\mathrm{Lsinh(d/L)}\}]$

In this table 2, $L = \sqrt{D\tau}$, $P = \frac{I_0\alpha L}{2D}$, $Z(x) = \frac{e^{-\alpha x} - e^{-x/L}}{1/L - \alpha} + \frac{e^{-\alpha x} - e^{x/L}}{1/L + \alpha}$, $Y(x) = e^{-\alpha d}\left\{\frac{e^{\alpha x} - e^{-x/L}}{1/L + \alpha} + \frac{e^{\alpha x} - e^{x/L}}{1/L - \alpha}\right\}$, $Z'(x) = dZ(x)/dx$ and $Y'(x) = dY(x)/dx$, respectively.

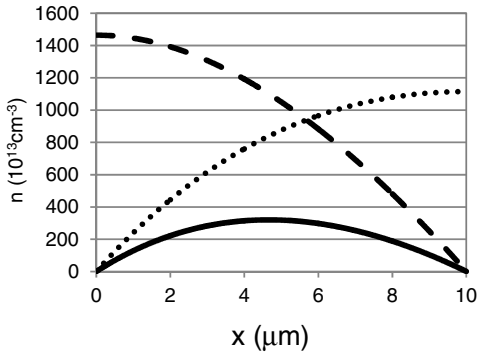

Figure 6. The calculated distribution of the electron density ($n(x)$) in TiO_2 films at short circuit condition for N-DSC (· · · · ··), BC-DSC(- - -) and SW-DSC(—). The α, d, n_0, D and τ values used for the calculations were 823 cm^{-1}, 10 μm, 10^{13} cm^{-3}, 5×10^{-4} cm^2 s^{-1} and 1 s, respectively. In this figure, light is irradiated from $x = 0$. The collection electrode in N-DSC and BC-DSC exists at $x = 0$ and d, respectively.

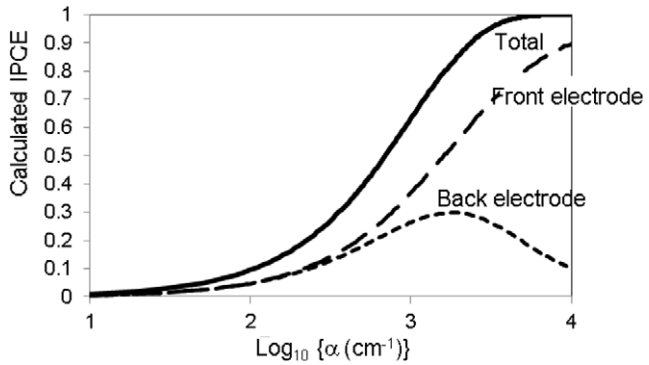

Figure 7. Absorption coefficient (α) dependent photocurrent density of the front collection electrode (- - -), the back collection electrode (· · · · ··) and total photocurrent density (—) calculated from equation (10). The following parameter values were used for the calculations: $d = 10\,\mu$m, $D = 9 \times 10^{-5}$ cm^2 s^{-1} and $\tau = 1$ s.

The collection electrode in N-DSCs, and BC-DSCs exists at $x = 0$ and d, respectively. According to the distribution of electrons in the TiO_2 of N-DSCs, the n value at $x = 0$ is smallest. The electron collection rate around the collection electrode was faster than the electron diffusion rate through the TiO_2 film. Therefore, the electron density decreased at the interface between the TiO_2 film and the electrode and an electron density gradient was generated around the collection electrode. The J_{SC} is determined by the diffusion rate, and not by the electron transfer rate (electron collection) at the interface between a TiO_2 film and a collection electrode in the diffusion model.

In BC-DSCs, electrons also diffuse to the collection electrode. The maximum n value in BC-DSCs is the largest in the three types of DSCs. In particular, the maximum n value in BC-DSCs is larger than that in N-DSCs. Electrons in TiO_2 are generated around the optical window ($x = 0$) of BC-DSCs. Electrons in TiO_2 have to transport from $x = 0$ to the back collection electrode ($x = d$). The AD of BC-DSCs is longer than that of N-DSCs. In addition, the D value in TiO_2 films is much smaller than that of bulk crystalline TiO_2. Therefore, electrons are accumulated around $x = 0$ in BC-DSCs when the τ is very large.

The maximum n value in SW-DSCs is smallest of the three types of DSC. In the TiO_2 film of an SW-DSC, the n at $x = 0$ and d were smallest because electrons are collected by the front and the back electrodes. The AD of SW-DSCs is shortest in these three structures. The electrons can quickly be collected as shown in figures 4 and 5. Therefore the maxmun n value in SW-DSCs is smallest at short circuit. The D and τ in DSCs depend on the electron density in TiO_2. In particular, the τ decreases in increase with n. The large n induces the charge recombination. Therefore, we assumed that the charge recombination can be minimized because of the small n in SW-DSCs.

In SW-DSCs, we assumed that the total current density can be expressed as the sum of the current densities at the front electrode and the back electrode for a given TiO_2 thickness d. In the diffusion model, we can estimate the contribution of the front and back electrodes to the collection of electrons in a TiO_2 film. We can separately calculate the photocurrent density as the following from equation (3):

$$J_{SC}^{F} = \frac{q I_0 \alpha}{2 \sinh(d/L)} Z(x = d), \tag{10a}$$

$$J_{SC}^{B} = \frac{q I_0 \alpha L}{2}\left(Z'(x = d) - Z(x = d)\frac{\cosh(d/L)}{L \sinh(d/L)}\right), \tag{10b}$$

where J_{SC}^{F}, and J_{SC}^{B} are the photocurrent density of the front and back electrodes, respectively. The value of $Z(x = d)$ and $Z'(x = d)$ are defined in table 2. The contribution of the J_{SC}^{F} and J_{SC}^{B} to the total photocurrent density can be estimated by changing the light absorption property as α (figure 7). The J_{SC}^{F} equals to J_{SC}^{B} below $\alpha = 100$. Many electrons can be generated at $x = d$ when the light is illuminated from $x = 0$

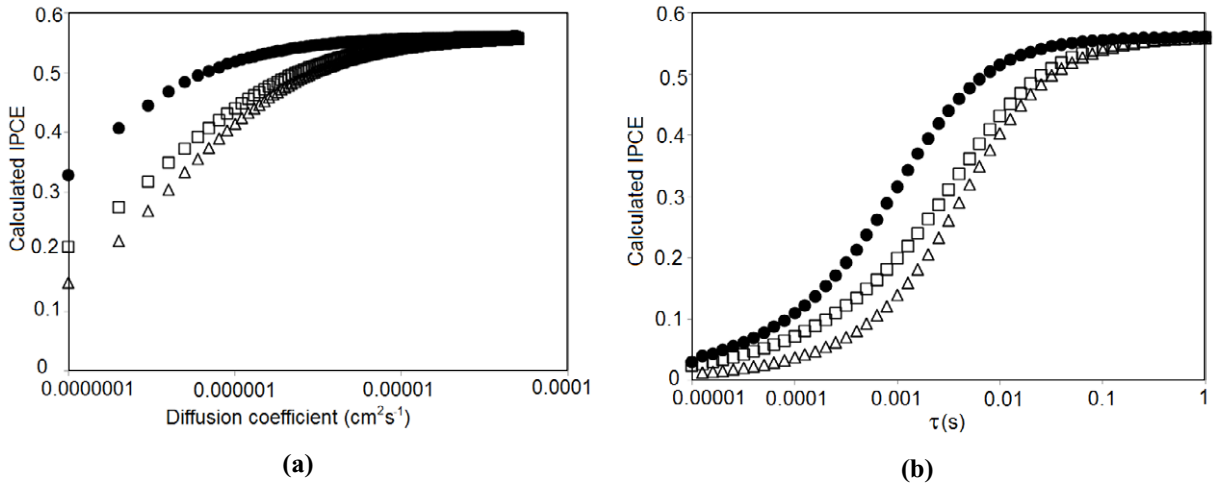

Figure 8. (a) Relationship between calculated IPCE and electron diffusion (D) of an N-DSC(□), a BC-DSC(△) and an SW-DSC (•). The α, d and τ values used for the calculations were 823 cm^{-1}, 10 μm and 1 s, respectively. (b) Relationship between calculated IPCE and electron lifetime (τ) of an N-DSC(□), a BC-DSC(△) and an SW-DSC (•). The α, d and D values used for the calculations were 823 cm^{-1}, 10 μm and 1×10^{-3} cm^2 s^{-1}, respectively.

as shown in figure 2. When the α increases over 100 cm^{-1}, electrons generated around $x = 0$ can be preferably collected by the front electrode. Therefore, the contribution of J_{SC}^{B} gradually decreases. Light harvesting efficiency of around 100% can be obtained at $x = 4/\alpha$ from equation (1). But J_{SC}^{B} is kept at around 10–20% of the total photocurrent density even when the value of $4/\alpha$ approaches the thickness of TiO_2 (10 μm). The contribution of J_{SC}^{B} is kept at around 10% even at $\alpha = 10^4$ cm^{-1}. The calculation means that electrons also diffuse from the front electrode to the back electrode even when α is large. The back electrode can effectively collect electrons in SW-DSCs.

3.5. The effect of the diffusion length

The diffusion length is the specific distance of electron transport in the medium, and can be expressed by $L = (D\tau)^{1/2}$. The long L is needed to improve the energy conversion efficiency of DCSs. The large D and long τ result in the long L. In this section, we investigated the effect of L on the properties of N-DSCs, BC-DSCs, and SW-DSCs.

Plots of the D dependence of the calculated IPCEs of the N-, BC- and SW-DSCs were comparable at $d = 10$ μm (figure 8(a)). The IPCE values increased with increasing D. The IPCE of the N- and BC-DSCs becomes smaller than that of the SW-DSC at D values $<10^{-5}$ cm^2 s^{-1}. The electrons in the TiO_2 film could not be efficiently collected by the front electrode in the N-DSC or the back electrode in the BC-DSC at $D < 10^{-5}$ cm^2 s^{-1} but could be collected by both the front and the back electrodes in the SW-DSC. Plots of the τ dependence of the IPCEs of the N-, BC- and SW-DSCs were comparable at $d = 10$ μm (figure 8(b)). The IPCE values increased with increasing τ. The IPCE of the SW-DSC was the largest of the three structures at $10^{-6} < \tau < 10^{-2}$ s. The electrons in the TiO_2 film could not be efficiently collected by the front electrode in the N-DSC or the back electrode in the BC-DSC at 10^{-4} s, but they could be collected by both the front and the back electrodes in the SW-DSC. The dependence of the calculated IPCEs on D and τ show that a high J_{SC} could be maintained when the electron diffusion length in the TiO_2 film was shortened.

4. Conclusion

We report the comparison for photocurrent density (J_{SC}) for N-, BC- and SW-DSCs to understand the role of structure of the electron collection electrode. Photocurrent response in SW-DSCs was the fastest of the three structures at frequencies between 10 and 500 Hz. We explained this difference in terms of the distance traveled by electrons in the conduction band of TiO_2: electrons far from the collection electrode had to diffuse for a long distance in N- and BC-DSCs, whereas in SW-DSCs, the electrons were collected by the front and back electrodes. In the SW-DSC, photogenerated electrons in the TiO_2 film were collected by both the front electrode and the back electrode. These results agreed with results calculated using the diffusion model.

In SW-DSCs, the average distance between the position of a photogenerated electron and an extraction electrode was half that in N- and BC-DSCs. The electron diffusion model shows electrons are effectively collected by the front and the back electrodes in SW-DSCs. The back electrode can effectively collect electrons in SW-DSCs even when α is large. Calculations based on the model suggested that a high short-circuit photocurrent could be maintained in SW-DSCs even when the electron diffusion length in the TiO_2 film was shortened.

Acknowledgments

This work was partially supported by Precursory Research for Embryonic Science and Technology (PRESTO) and Core Research for Evolutional Science and Technology (CREST) of Japan Science and Technology agency. This preparation of the back electrode was supported by Nano-Integration Foundry (NIMS) in 'Nanotechnology Platform Project' operated by the Ministry of Education, Culture, Sports, Science and Technology (MEXT), Japan. The authors

gratefully acknowledge the kind help for the preparation of devices by Mr Takeshi Sugita, Mr Masayuki Chikatsu, Ms Naomi Itoh and Ms Toshiko Harimoto.

References

[1] O'Regan B and Grätzel M 1991 *Nature* **353** 737
[2] Nazeeruddin Md K, Kay A, Rodicio I, Humphry-Baker R, Müller E, Liska P, Vlachopoulos N and Grätzel M 1993 *J. Am. Chem. Soc.* **115** 6382
[3] Nazeeruddin Md K *et al* 2001 *J. Am. Chem. Soc.* **123** 1613
[4] Hagfeldt A and Grätzel M 1995 *Chem. Rev.* **95** 49
[5] Hagfeldt A, Boschloo G, Sun L, Kloo L and Pettersson H 2010 *Chem. Rev.* **110** 6595
[6] Chiba Y, Islam A, Watanabe Y, Komiya R, Koide N and Han L 2006 *Japan. J. Appl. Phys.* **45** L638
[7] Han L, Islam A, Chen H, Malapaka C, Chiranjeevi B, Zhang S, Yang X and Yanagida M 2012 *Energy Environ. Sci.* **5** 6057
[8] Green M A, Emery K, Hishikawa Y, Warta W and Dunlop E D 2012 *Prog. Photovolt., Res. Appl.* **20** 12
[9] Yanagida M, Onozawa-Komatsuzaki N, Kurashige M, Sayama K and Sugihara H 2010 *Sol. Energy Mater. Sol. Cells* **94** 297
[10] Södergren S, Hagfeldt A, Olsson J and Lindquist S-E 1994 *J. Phys. Chem.* **98** 5552
[11] Dloczik L, Ileperuma O, Lauermann I, Peter L M, Ponomarev E A, Redmond G, Shaw N J and Uhlendorf I 1997 *J. Phys. Chem.* B **101** 10281
[12] Kern R, Sastrawan R, Ferber J, Stangl R and Luther L 2002 *Electrochim. Acta* **47** 4213
[13] Duffy N W, Peter L M, Rajapakse R M G and Wijayantha K G U 2000 *J. Phys. Chem.* B **104** 8916
[14] Duffy N W, Peter L M, Rajapakse R M G and Wijayantha K G U 2002 *Electrochem. Commun.* **2** 658
[15] Peter L M, Ponomarev E A, Franco G and Shaw N J 1999 *Electrochim. Acta* **45** 549
[16] Cai J and Han L 2011 *J. Phys. Chem.* C **115** 17154
[17] Yanagida M, Miyamoto K, Sayama K, Kasuga K, Kurashige M, Takano S, Fujihashi G, Abe Y and Sugihara H 2006 *Electrochim. Acta* **51** 3993
[18] Boschloo G, Häggman L and Hagfeldt A 2006 *J. Phys. Chem.* B **110** 13144
[19] Schlichthörl G, Park N G and Frank A J 1999 *J. Phys. Chem.* B **103** 782
[20] Nakade S, Saito Y, Kubo W, Kitamura T, Wada Y and Yanagida S 2003 *J. Phys. Chem.* B **107** 8607
[21] Kopidakis N, Schiff E A, Park N-G, van de Lagemaat J and Frank A J 2000 *J. Phys. Chem.* B **104** 3930
[22] Cao F, Oskam G, Meyer G J and Searson P C 1996 *J. Phys. Chem.* **100** 17021
[23] Fuke N, Fukui A, Komiya R, Islam A, Chiba Y, Yanagida M, Yamanaka R and Han L 2008 *Chem. Mater.* **20** 4974
[24] Fuke N *et al* 2009 *Energy Environ. Sci.* **2** 1205
[25] Fuke N, Fukui A, Chiba Y, Komiya R, Yamanaka R and Han L 2007 *Japan. J. Appl. Phys.* **46** L420
[26] Fuke N, Fukui A, Islam A, Komiya R, Yamanaka R, Han L and Harima H 2008 *J. Appl. Phys.* **104** 064307
[27] Lobato K, Peter L M and Würfel U 2006 *J. Phys. Chem.* B **110** 16201
[28] Lobato K and Peter L M 2006 *J. Phys. Chem.* B **110** 21920
[29] Würfel U, Peters L M and Hinsch A 2008 *J. Phys. Chem.* C **112** 1711
[30] Zhang S, Yanagida M, Yang X and Han L 2011 *Appl. Phys. Express* **4** 042301
[31] Zhang S, Yang X, Zhang K, Chen H, Yanagida M and Han L 2011 *Phys. Chem. Chem. Phys.* **13** 19310
[32] Fu D, Zhang X L, Barber R L and Bach U 2010 *Adv. Mater.* **22** 4270
[33] Yoo B, Kim K-J, Kim Y H, Kim K, Ko M J, Kim W M and Park N-G 2011 *J. Mater. Chem.* **21** 3077
[34] Yoo B, Kim K-J, Lee D-K, Kim K, Ko M J, Kim Y H, Kim W M and Park N-G 2010 *Opt. Express* **18** A395
[35] Kashiwa Y, Yoshida Y and Hayase S 2008 *Appl. Phys. Lett.* **92** 033308
[36] Beppu T, Kashiwa Y, Hayase S, Kono M and Yamaguchi Y 2009 *J. Appl. Phys.* **48** 061504
[37] Kroon J M *et al* 2007 *Prog. Photovolt., Res. Appl.* **15** 1
[38] Yanagida M, Numata Y, Yoshimatsu K, Ochiai M, Naito H and Han L 2013 *Electrochim. Acta* **87** 309
[39] Koide N, Chiba Y and Han L 2005 *Japan. J. Appl. Phys.* **44** 4176
[40] Koide N and Han L 2004 *Rev. Sci. Instrum.* **75** 2828